CFSRC COLLOQUIUM

Proceedings of the Cold-Formed Steel Research Consortium Colloquium
20-22 October 2020 (cfsrc.org)

Stiffness Characterization of Single Lap Shear Screw Fastened Connections Using Finite Element Modeling

Rita Kalo[1], Kara Peterman[2]

Abstract

Cold-formed steel (CFS) connections are commonly fastened using self-tapping self-drilling screws. Though screw manufacturers typically provide the strength of their screws, the stiffness of these connections is typically not reported. While modern design codes are strength-based, stiffness is increasingly necessary to characterize cold-formed steel system response in seismic applications. The full force-displacement response of the fastened connections is required for energy dissipation analysis. Historically, researchers and engineers have conducted experimental testing to determine connection behavior. However, repeatedly conducting this type of experiment is time consuming and expensive. This work aims to create robust finite element models that can successfully predict the force-displacement response of single lap steel-to-steel shear connections, without requiring tests. Five models of single lap screw connections were created using the finite element program ABAQUS/CAE. The thickness of the two CFS plies used in the connection varied for each model. These models were validated using experimental results of identical screw connections. Stiffness is the focus of the work herein, though strength results are also provided. During the development of the models, it was found that the contact parameters defined between the screw and the CFS plies had the most significant effect on the connection stiffness. To further investigate the effect of each contact parameter on the stiffness of the models, a parametric study was also conducted. In general, the results of the modelling program showed good agreement with the stiffness found in the tests. This work represents a promising first step in finite element characterization of cold-formed steel fastened connections.

1. Introduction

Cold-formed steel (CFS) structures have been the subject of much research in recent years. Unique to light-framed construction is the critical role fastener behavior plays in dictating sub-system and even system-level response. This has been identified in research by Bian et. al [1] and Leng et. al [2]. Though bolted and welded connections have been modeled by researchers at length in hot-rolled steel and cold-formed steel structures, the same is not true for screw-fastened CFS connections.

The available research on CFS screw fastened connections is frequently based on experimental testing [3-5], or primarily strength based [6-7]. While strength limit states are acceptable for capacity-design, the response of CFS systems to seismic loading requires the stiffness of individual connections to be characterized. This has been achieved in the past by performing tests for individual connections under monotonic and cyclic loads [8]. However, repeatedly conducting such tests can be time consuming and expensive. Furthermore, continuous innovation in the construction market results in a plethora of new products with new structural configurations. Simply put, while there is a wealth of experimental data, it is difficult to find the exact configurations that might be specified in a given structural design. Therefore, the purpose of this work is to develop finite element models of screw fastened CFS connections that can predict the stiffness, peak load, and failure mode of the connection. Each model was validated using experimental results of identical connections, with the final goal of this research being to shift away from the use of any tests for model validation or calibration.

2. Model and Test Setup

The models were created using ABAQUS/Standard in the finite element program ABAQUS CAE, version 6.14. The setup of the models is based on tests conducted by Pham and Moen [9] of single lap shear screw fastened connections. Two 152x203 mm (6 inches x 8 inches) CFS plies are fastened together with a hex head self-tapping self-drilling screw (Simpson X Screw). Five models were created with this setup, each using a #10, or 4.826 mm (0.19in) diameter screw. The thicknesses of the CFS plies differed for each test. A schematic of the test setup can be seen in

[1] Structural Engineer and former Graduate Student Researcher at UMass Amherst, PRIME AE Group, Inc., r.kalo@hotmail.com
[2] Assistant Professor, Department of Civil & Environmental Engineering, UMass Amherst, kdpeterman@umass.edu

Figure 1a. Each ply is bolted to an aluminum fixture to restrict out of plane motion during testing. Both fixtures have a 102x102mm (4.02x4.02 inches) opening where the plies are not restrained. These boundary conditions in the tests are designed to create behavior in the plies similar to a "web stiffened by flanges" [9] as can be seen in Figure 1b. The ply in contact with the screw head – ply 1 – is bolted to the movable fixture where load is applied in monotonic displacement control until failure at a speed of 0.025mm/s (0.001in/s). The other ply – ply 2 – is bolted to another fixture that is fixed.

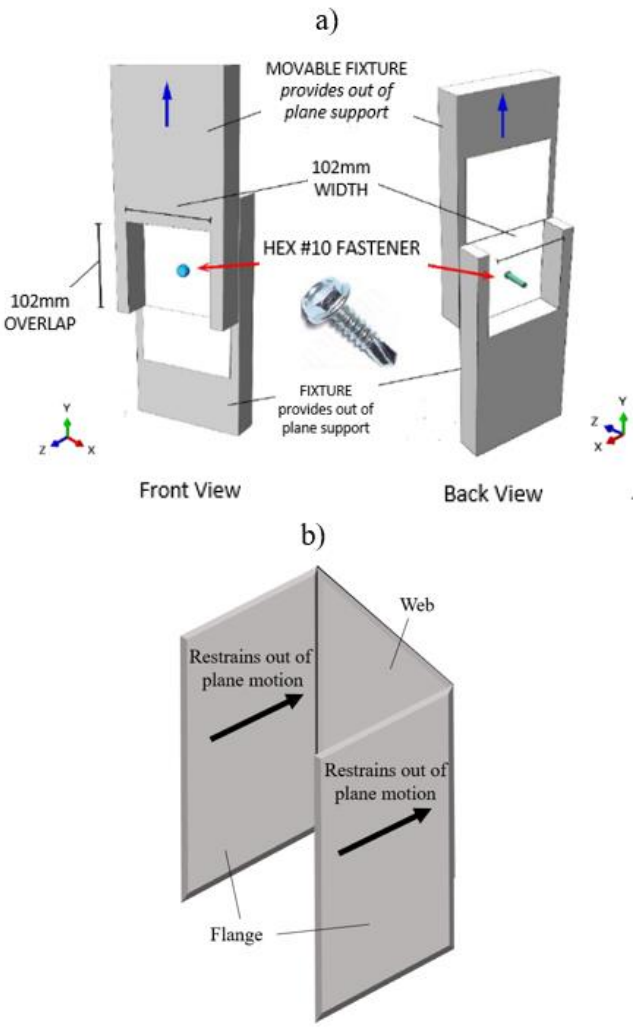

Figure 1: a) Schematic of test setup adapted from Corner [10] b) Out of plane motion behavior on a CFS channel

To track the movement of the connection, measurements were taken at three target points that can be seen on Figure 2. Measurement 1 was taken at the center of the screw head to measure the angle of the screw during testing. Measurements 2 and 3 were taken on plies 1 and 2 to track the relative displacement of the screw. Measurement 2 is taken 114mm (4.49 inches) above the bottom of ply 1, and measurement 3 is taken 25.4mm (1 inch) below the top of ply 2. The difference between measurements 2 and 3 during loading is the relative displacement of the connection. The stiffness of the connection is calculated based on the relationship between the applied force on the movable fixture and the relative displacement between the plies.

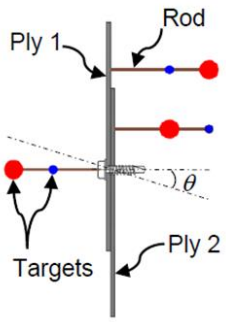

Figure 2: Schematic of test and model measurement points [9]

To simplify each model, the aluminum fixtures used in the tests were not added to the model. Instead, the effect of the aluminum fixtures was created using boundary conditions on the plies. In Figure 3, the boundary conditions of the model can be seen in shaded purple and restrict out of plane motion. Upward motion is also restrained at the bottom of ply 2.

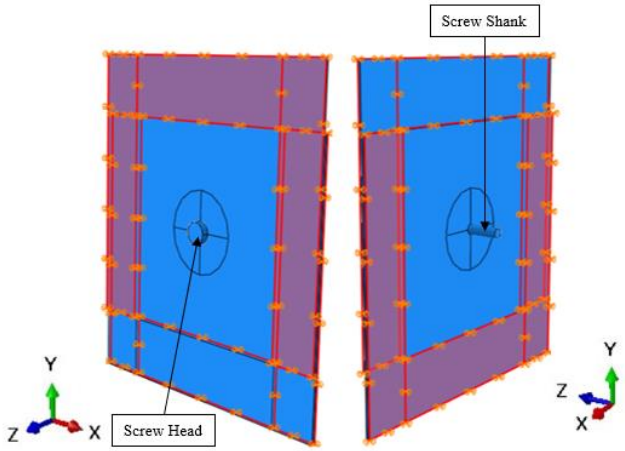

Figure 3: Model setup and boundary condition locations on model [11]

The screw modeling also differed from the screw used in the tests. The hex head and washer of the screw was replaced with a circular head with no washer, and a smooth screw shank was modeled instead of incorporating the threads. Because the connections modeled are shear connections, the specific shape of the head has a negligible effect on the behavior of the connection. A smooth screw shank was used to simplify the mesh required for the shank. Very complex meshing and contact definitions would be required to successfully model the

screw threads. Instead, the effect of the screw threads was accounted for with changes to the default contact definitions between the shank and the holes in each CFS ply. Figure 4 below shows the differences between the self-drilling screw used in the tests (Figure 4b) and the screw used in the models (Figure 4a). The thickness and diameter of the screw head used in the tests were maintained in the screw model. The length of the Simpson X Screw shank is a minimum of 25.4 mm (1 inch) per the ICC Evaluation Service [12]. The shank length in the model was reduced to 19.05 mm (0.75 inches) [11], as this decreased the total run time of each model while having an insignificant effect on the results.

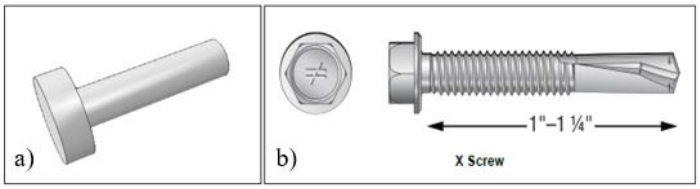

Figure 4: a) Screw model in ABAQUS b) Simpson X Screw used in tests [12]

The modeling of the plies had only one difference compared to the tests – their length. It was found that modeling the entire length of each ply used in the test significantly increased the run time of each model but had negligible effects on the behavior of the connection. Therefore, the plies in each model had the same thicknesses and width as their corresponding test, but were 132 mm long (5.20 inches) [11] in the model instead of 203 mm (8 inches) like the test.

The test and model matrix is in Table 1. The model name is the nominal thickness of ply 1 in mils, followed by the nominal thickness of ply 2 in mils. For example, the 33-68 model has a ply 1 of 33 mils and a ply 2 of 68 mils.

Table 1: Test and Model Matrix

Model Name	Ply 1 Measured Thickness in mm (in)	Ply 2 Measured Thickness in mm (in)
33-33	0.88 (0.0346)	0.88 (0.0346)
43-43	1.19 (0.0469)	1.19 (0.0469)
33-68	0.89 (0.0350)	1.81 (0.0713)
43-54	1.19 (0.0469)	1.40 (0.0551)
43-68	1.19 (0.0469)	1.83 (0.0720)

3. Contact Parameters

In the models, a hard-normal contact relationship was defined between the plies and the screw. The default settings of this contact relationship result in minimal penetration between two surfaces in contact. The contact parameters in ABAQUS had the strongest effect on the behavior of the model. Due to the threads on the screw shank being excluded from the model, a default hard normal contact relationship can artificially increase the strength and stiffness of the connection. This increased stiffness is similar to bolted connections where minimal penetration between the bolt shank and the bolt hole is expected. Bolted connection models that use a smooth shank and default contact parameters have shown good agreement with test results by other researchers [13-14]. However, bolted connections are much stiffer than screw fastened connections, so the contact relationship must be modified from the default to produce the correct connection behavior in each model.

The contact parameters changed for each model are the minimum contact stiffness (K_i), the maximum contact stiffness (K_f), the lower quadratic limit (e) and the upper quadratic limit (d). The relationship between these parameters can be seen in Figure 5. The lower and upper quadratic limits are the amounts of penetration allowed between contact surfaces per the ABAQUS Analysis User's Guide [15]. The lower quadratic limit is the maximum penetration allowed between surfaces before the contact stiffness increases from K_i. The upper quadratic limit is the maximum penetration allowed before the contact stiffness reaches K_f and remains constant. The effect of each parameter on the behavior of the model is discussed in the following sections.

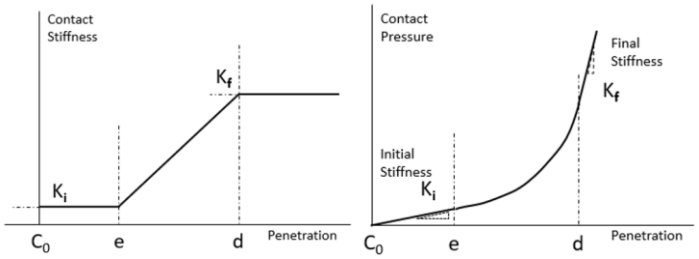

Figure 5: Relationship between hard-normal contact parameters in ABAQUS (adapted from ABAQUS Analysis User's Guide 2014 [15])

3.1 Parametric Study – Maximum and Initial Contact Stiffness

Maximum contact stiffness K_f has the most significant effects on three aspects of the models: the connection stiffness, the final displacement of the model before failure, and the peak load. To minimize penetration, the default K_f in ABAQUS is a very high value. If this value is used, the connection stiffness, final displacement (before failure of the connection), and peak load of the model are at their highest possible values. This means that using the default contact stiffness consistently produces an overly stiff

model. Therefore, each model required the K_f to be reduced to reduce the stiffness of the connection. Figure 6a demonstrates this effect. Using the low K_f in the model results in a much lower final displacement, and a significantly lower connection stiffness than the high K_f and default K_f. The low K_f is 2 kN/mm^3 (7368 kip/in^3), and the high K_f is 10 kN/mm^3 (36841 kip/in^3) [11]. Since the default K_f is controlled by ABAQUS, its exact value is not available to view within the program, but has a greater magnitude than the high K_f.

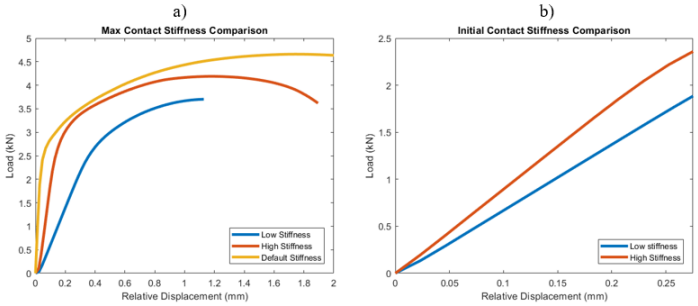

Figure 6: a) Effect of K_f on connection stiffness of models [11] b) Effect of K_i on connection stiffness of models [11]

The initial contact stiffness K_i has the strongest effect on the initial connection stiffness of the model. In the Pham and Moen [9] tests, the stiffness of the connections was measured when the load is at 40%, 80% and 100% of the peak load. In the model results, the stiffness at 40% of peak load is the “initial connection stiffness”. In Figure 6b, a comparison of initial connection stiffnesses in the same model can be seen when the K_i value changes. A higher K_i results in a higher initial stiffness, and a lower K_i results in a lower connection stiffness. In the figure, the high K_i is 3.60 kN/mm^3 (13,262 kip/in3), and the low K_i is 2.25 kN/mm^3 (8289 kip/in^3) [11].

Because the contact stiffness is designed in ABAQUS to gradually increase as force (or contact pressure) increases in the two surfaces in contact, K_i must be low enough to ensure that K_f is only reached after yielding begins to occur in the screw or plies. If yielding has not occurred before the contact stiffness is equal to K_f, the connection stiffness will significantly increase after the 40% of peak load point. This is because without yielding of the connection components, there is no strength degradation in the connection to reduce the stiffness before peak load is reached.

3.2 Parametric Study – Lower and Upper Quadratic Limits

The lower quadratic limit, or *e* in ABAQUS, controls the amount of penetration allowed between surfaces in contact while the contact stiffness remains constant and equal to K_i [15]. Even if the K_i and K_f values are changed from their defaults, the connection behavior can still revert to its natural overly stiff behavior once K_f is reached. This is because a high contact stiffness creates a high connection stiffness. By increasing *e* from its default, more penetration will be allowed before the contact stiffness starts to increase beyond K_i. This can prevent the connection stiffness from increasing before the plies reach yield.

This can be seen in Figure 7. The *e* value is changed in ABAQUS via a ratio of *e/d.* The low penetration and high penetration ratios in the Figure 7 curves are 0.67 and 0.99 [11]. The low penetration curve in blue has a lower *e* value than the red high penetration curve. Both stiffness curves begin with the same connection stiffness, but the low penetration line has an increase in stiffness that occurs at a lower relative displacement (between the two plies) than the high penetration line.

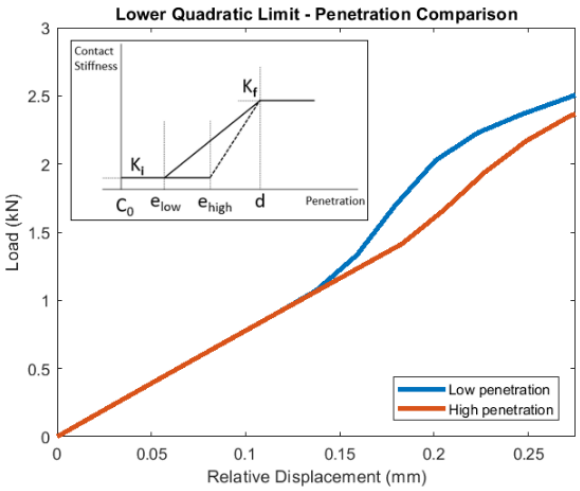

Figure 7: Effect of *e* on connection stiffness [11]

After the upper quadratic limit *d* is reached, the contact stiffness remains constant and equal to K_f [15]. To maintain the desired stiffness in the models, *d* must be set to a sufficiently high value to ensure that the connection stiffness does not sharply increase. If *d* is at an appropriate value, the connection stiffness will soften due to material yielding prior to the contact surfaces reaching a penetration *d.* In Figure 8 below, the effects of using a low, medium and high *d* value in the same model are compared.

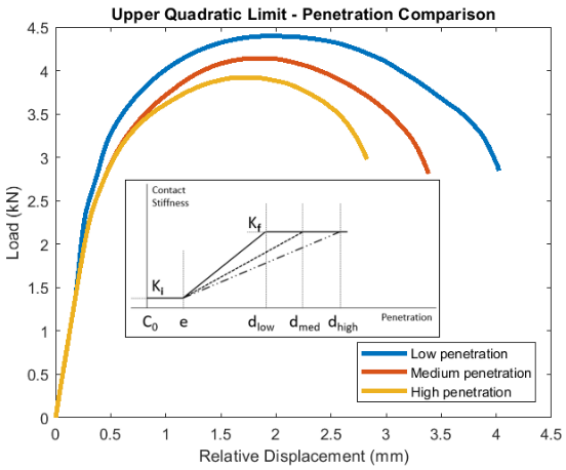

Figure 8: Effect of *d* on connection stiffness [11]

To control *d* in the models, the value is scaled by the "upper quadratic limit scale factor" in ABAQUS. The low *d* has a factor of 0.2, the medium *d* has a factor of 0.35, and the high *d* has a factor of 0.5 [11]. The curve corresponding to the high penetration *d* has the smoothest stiffness curve compared to the low and medium penetration curves. Based on the behavior of the high penetration curve, the model components begin to yield prior to reaching penetration *d* between the two surfaces, resulting in a consistent connection stiffness. Before reaching peak load, the low penetration curve has a visible increase in connection stiffness before the plies begin to yield and the stiffness decreases again.

4. Results

All the models failed due to a combination of screw tilting and ply bearing. This corresponds with the failure mode seen in the tests. The holes in both plies have exceeded their yield strength, and significant tilting can be seen in the screw. This typical behavior in the models can be seen in the 33-33 model results shown in Figure 9 [11].

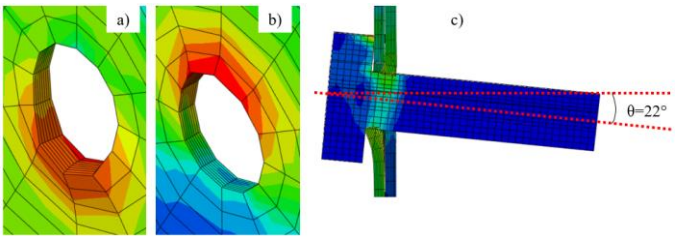

Figure 9: 33-33 failure mode a) Ply 1 hole b) Ply 2 hole c) Screw tilting

The overall stiffness and peak load results are found in Figure 10. As can be seen in Figure 10, the peak load for each model showed good agreement with the tests. For example, the average peak load per Pham and Moen [9] was 3.07 kN (690.16 lbs) for the 33-33 tests, while the model peak load was 2.95 kN (663.18 lbs) [11].

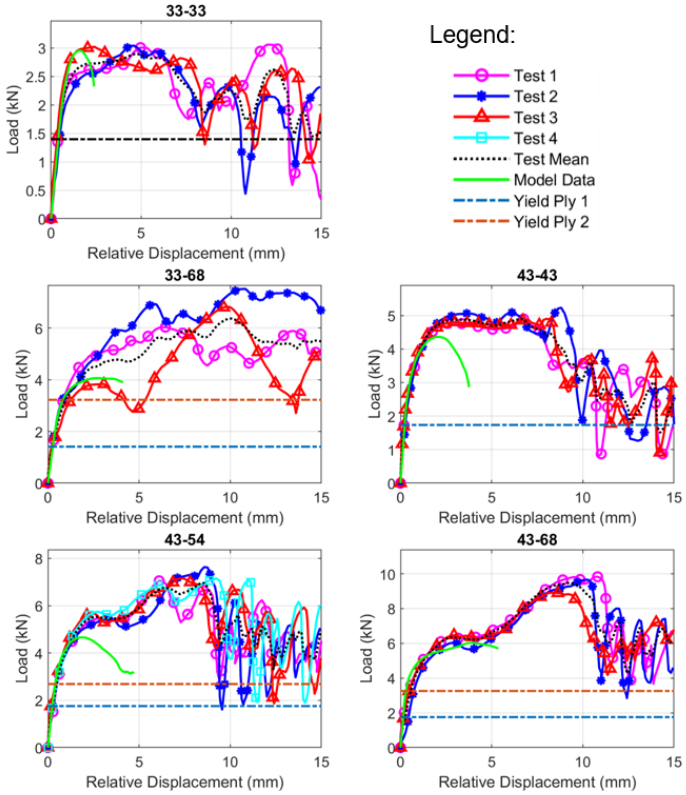

Figure 10: Overall model results vs test results

The connection stiffness of all models is compared to their corresponding tests in Table 2 at 40%, 80% and 100% of peak load. For all models, the connection stiffness at 40% of peak load showed good agreement with the tests. The stiffness at 80% and 100% of peak load are consistently higher than the test results. Between 40% and 80% of peak load, the stiffness decreases by over 55-60% for each test. In the models, the connection stiffness typically decreases by less than 55%. This discrepancy between the models and the tests is likely due to the changes in contact stiffness that occur between 40% and 80% of peak load.

In each model, 80% of peak load is the approximate point where contact stiffness K_f is reached. This means that although yielding of the plies has somewhat reduced the stiffness of the connection, the connection behavior is still reverting to becoming overly stiff. The result of this is a higher connection stiffness at 80% and 100% of peak load in each model compared to the tests.

Table 2: Model stiffness results vs test results

Test	% of Peak Load	Model kN/mm (kip/in)	Test Mean kN/mm (kip/in)	Percent Difference (%)
33-33	40	3.46 (19.76)	4.21 (24.04)	17.8%
	80	2.77 (15.82)	1.69 (9.67)	63.9%
	100	0.730 (4.16)	0.283 (1.62)	1.58%
43-43	40	7.68 (43.85)	8.05 (45.95)	4.5%
	80	3.44 (19.64)	2.74 (15.66)	25.5%
	100	0.610 (3.48)	0.470 (2.66)	29.8%
33-68	40	5.21 (29.75)	4.65 (26.55)	12.0%
	80	3.14 (17.93)	1.07 (6.13)	193%
	100	0.440 (2.51)	0.500 (2.87)	12.0%
43-54	40	7.21 (41.17)	8.29 (47.32)	13.0%
	80	4.17 (23.81)	2.75 (15.68)	51.6%
	100	0.820 (4.68)	0.657 (3.75)	24.8%
43-68	40	6.92 (39.51)	8.78 (50.14)	21.2%
	80	5.59 (31.92)	3.13 (17.89)	78.6%
	100	0.840 (4.80)	0.870 (4.99)	3.45%

5. Conclusions

In this work, models were created that can successfully characterize the stiffness of screw fastened connections. Through changes to contact parameters between the cold-formed steel plies and the screw, the initial stiffness of model connections showed good agreement with their corresponding tests. The peak load and failure mode of each model also matched the tests, further confirming the accuracy of the models. This work is a promising first step to reducing the use of experimental tests to characterize the stiffness of cold-formed steel screw fastened connections.

References

[1] Bian, G., Padilla-Llano, D. A., Leng, J., Buonopane, S. G., Moen, C. D., & Schafer, B. W. (2015). OpenSees modeling of cold formed steel framed wall system. *8th International Conference on Behavior of Steel Structures in Seismic Areas.* Shanghai, China.

[2] Leng, J., Buonopane, S. G., & Schafer, B. W. (2016). Seismic Modeling and Incremental Dynamic Analysis of the Cold-Formed Steel Framed CFS-NEES Building. *International Specialty Conference on Cold-Formed Steel Structures.* St. Louis, MO.

[3] Peterman, K. D., Nakata, N., & Schafer, B. W. (2014). Hysteretic characterization of cold-formed steel stud-to-sheathing connections. *Journal of Constructional Steel Research*, 254-264.

[4] Fülöp, L. A., & Dubina, D. (2004). Performance of wall-stud cold-formed shear panels under monotonic and cyclic loading Part I: Experimental research. *Thin-Walled Structures*, 321-338.

[5] Fiorino, L., Della Corte, G., & Landolfo, R. (2007). Experimental tests on typical screw connections for cold-formed steel housing. *Engineering Structures*, 1761-1773.

[6] Ye, J., Feng, R., Chen, W., & Liu, W. (2016). Behavior of cold-formed steel wall stud with sheathing subjected to compression. *Journal of Constructional Steel Research*, 79-91.

[7] Nithyadharan, M., & Kalyanaraman, V. (2011). Experimental study of screw connections in CFS-calcium silicate board wall panels. *Thin-Walled Structures*, 724-731.

[8] Lin, S.-H., Pan, C.-L., & Hsu, W.-T. (2014). Monotonic and cyclic loading tests for cold-formed steel wall frames sheathed with calcium silicate board. *Thin-Walled Structures,* 49-58.

[9] Pham, H. S., & Moen, C. D. (2015). Stiffness and Strength of Single Shear Cold-Formed Steel Screw-Fastened Connections. Blacksburg, Virginia.

[10] Corner, S. M. (2014). Screw-Fastened Cold-Formed Steel-to-Steel Shear Connection Behavior and Models. *Master's Thesis*. Blacksburg, Virginia.

[11] Kalo, R. (2019). High Fidelity Modeling of Cold-Formed Steel Single Lap Shear Screw Fastened Connections. *Master's Thesis*.

[12] ICC Evaluation Service. (2018, November 27). Simpson Strong-Tie Strong-Drive X and FPHSD Self-Drilling Tapping Screws. Retrieved from icc-es.org: https://www.icc-es.org/wp-content/uploads/report-directory/ESR-3006.pdf

[13] Kim, T. S., Kuwamura, H., & Cho, T. J. (2008). A parametric study on ultimate strength of single shear bolted connections with curling. *Thin-Walled Structures*, 38-53.

[14] Salih, E. L., Gardner, L., & Nethercot, D. A. (2010). Numerical investigation of net section failure in stainless steel bolted connections. *Journal of Constructional Steel Research*, 1455-1466.

[15] Dassault Systèmes. (2014). Abaqus Analysis User's Guide 6.14. Providence, Rhode Island: Abaqus FEA.